



cambridge.org/mrf

Carmine Mustacchio<sup>1</sup> , Emilio Arnieri<sup>1</sup> , Giandomenico Amendola<sup>1</sup>,  
Alessandro Fonte<sup>2</sup>, Riccardo Maggiora<sup>3</sup> and Luigi Boccia<sup>1</sup>

<sup>1</sup>MAIC Lab: Dipartimento di Ingegneria Informatica, Modellistica, Elettronica e Sistemistica (DIMES), Università della Calabria, Rende, Italy; <sup>2</sup>Microwave Components Research and Development Laboratories, SIAE Microelettronica, Cologno Monzese, Italy and <sup>3</sup>Department of Electronics and Telecommunications, Politecnico di Torino, Turin, Italy

Present address: Carmine Mustacchio; ST Microelectronics; Grenoble, France

## Research Paper

**Cite this article:** Mustacchio C, Arnieri E, Amendola G, Fonte A, Maggiora R, Boccia L (2024) E-band backhaul antenna for fine beam alignment. *International Journal of Microwave and Wireless Technologies* **16**(1), 30–40. <https://doi.org/10.1017/S1759078723000788>

Received: 06 February 2023  
Revised: 30 May 2023  
Accepted: 01 June 2023

### Keywords:

antenna design; modeling and measurements; system applications and standards

### Corresponding authors:

Carmine Mustacchio;  
Email: [c.mustacchio@dimes.unical.it](mailto:c.mustacchio@dimes.unical.it);  
Luigi Boccia; Email: [luigi.boccia@unical.it](mailto:luigi.boccia@unical.it)

### Abstract

An E-band Cassegrain switched beam high-gain antenna concept for 5G backhauling systems is proposed in this article. The antenna requirements target the compensation of small misalignments (within  $\pm 1$  degrees in both azimuth and elevation planes) in E-band backhauling links due to adverse weather conditions or thermal deformations. The intended antenna is able to realize beam-switching operations by using a feed-array architecture based on a  $7 \times 7$  array of cavity-backed magnetoelectric (ME) dipoles, where every element is capable of providing a steering of  $\pm 0.33$  degrees in both the elevation and the azimuth planes. The ME dipole illuminators combined with a Cassegrain reflector provide a gain of 52 dBi within the whole scanning range. Besides, they can be easily integrable with the front-end modules, thus being an easily implementable and low-cost alternative to other more complex solutions based on horns or lens antennas.

## Introduction

Backhauling links are receiving increasing attention as they play a main role in sustaining the huge fronthaul data rate, as they represent the interconnections between the core of a telecommunication network and its peripheral nodes (e.g., base stations) [1]. Among the spectrum portions for backhauling for 5G applications, the E-band (71–86 GHz) is one of the most interesting and attractive. In this frequency range, atmospheric losses and path attenuation make long-range communication links very difficult to achieve. In this context, antennas play a crucial role [2]. Point-to-point E-band backhaul links require high-gain antennas (ETSI 38 dBi and FCC 43 dBi). The resulting half power beamwidth (HPB) comprises between 1 and 2 degrees, thus requiring stable masts which have to provide high mechanical rigidity (Fig. 1). Even so, the thermal deformations as well as wind generate twists and sways in the order of 1 degree in both azimuth and elevation planes [3]. Therefore, E-band backhaul antenna systems should be capable to compensate mast movements to reduce the risk of outage. Several solutions were proposed to overcome these issues. Phased arrays, although representing a technically viable solution, are expensive and power consuming for such applications [4]. Several alternative solutions were proposed, the most common being the integration of fixed-beam antennas with a mechanical pointing system. In this configuration, different types of antennas can be used. For instance, high directivity can be fulfilled by using conventional lens [5, 6] or reflector antennas [7, 8]. However, high attention is deserved to antennas having low-cost beam pointing systems, which are based on electronic systems, preferable also because of the faster pointing speed. One option to achieve the beam steering requirements is to use Rotman lenses [9] combined with a switching system. Although several solutions of this type were proposed in literature [10], the implementation of such systems for the application at hand is not easy for two reasons. First, the implementation of 2D beam steering requires complex integration of the Rotman lenses. Second, Rotman lenses are difficult to be designed for tight scanning angles. An alternative solution was proposed using a 64 array of patches integrated with a lens [5]. Such a solution provides a gain of 36 dBi and  $\pm 4$  and  $\pm 17$  degrees of scanning in the azimuth and elevation planes, respectively. However, the latter configuration cannot be easily adaptable to higher gain architectures.

In this paper, a novel antenna architecture for E-band backhauling applications is introduced. The proposed solution combines a high-gain Cassegrain reflector antenna with a printed feed array. Feed array reflectors are typically employed in satellite communications to provide multi-spot Earth coverage [11]. Conversely, the envisioned solution employs a feed array architecture to realize beam-switching operations in 2D. The proposed feed array solution is based on a  $7 \times 7$

© The Author(s), 2023. Published by Cambridge University Press in association with the European Microwave Association





Figure 1. Cassegrain reflector antenna with small boom movements.

Table 1. Main antenna requirements

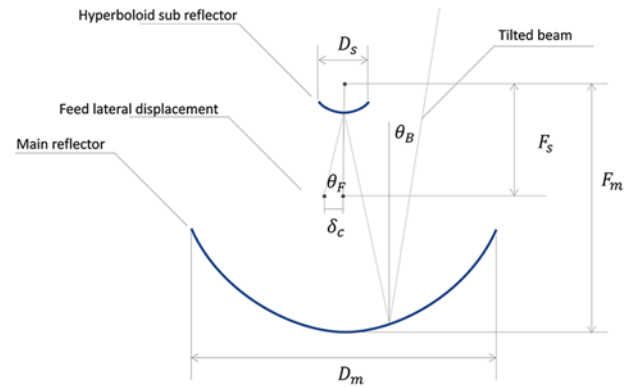
Requirements	Value
Frequency range	71–76 GHz to 81–86 GHz
Steering range	$\pm 1^\circ$
Gain	$\geq 50$ dBi
Polarization	Linear

array of printed elements. The use of a printed solution is essential to guarantee easy integration with the monolithically integrated front-ends. In order to provide the required gain and beamwidth, the printed feeds were realized by designing and testing cavity-backed magnetoelectric (ME) dipoles whose preliminary results were introduced in [12]. In this work, previous results are expanded by including a comprehensive experimental assessment and by introducing the integration with the Cassegrain reflector.

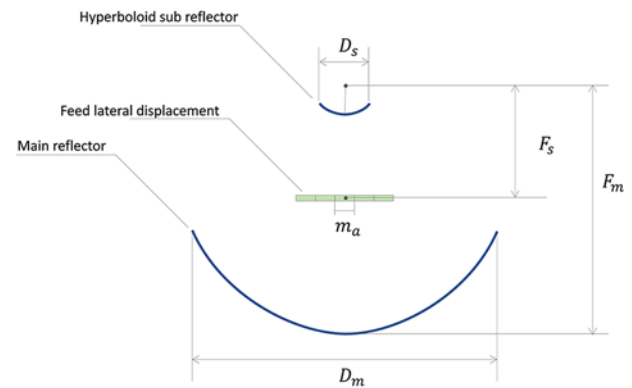
**Beam-switched Cassegrain antenna concept**

The most pertinent E-band antenna requirements for the back-hauling application at hand are summarized in Table 1.

Steering of the beam is required within the range of  $\pm 1$  degrees in both the azimuth and elevation planes. The antenna bandwidth should include both Tx and Rx channels, resulting in coverage from 71 to 86 GHz. Across the bandwidth and within the scanning range, a gain of higher than 50 dBi should be achieved with linear polarization. As a result of such requirements, several solutions have been investigated and compared, ultimately leading to the selection of a double-reflector configuration combined with a feed array. The proposed configuration is illustrated in Fig. 2a. Each feed occupies an area of  $m_a \times m_a$  and, in production, is connected to a chip implementing Tx and Rx functions. The central feed element is aligned with the reflector axis. By activating an axially displaced feed, the reflector beam points toward an angle  $\theta_B$ . Therefore, the integration of each feed of the board with



(a)



(b)

Figure 2. Multi-feed Cassegrain reflector antenna concept.

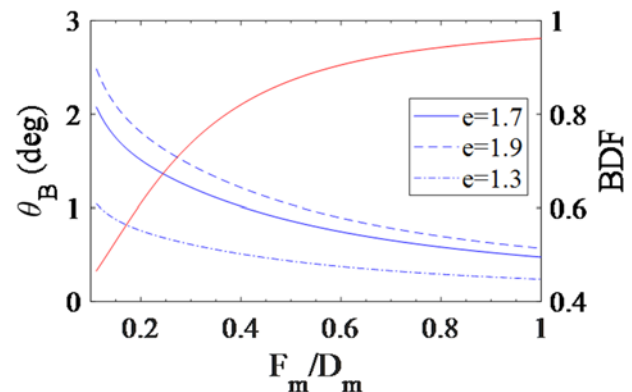


Figure 3. Lateral feed displacement effects as a function of  $F/D$ : red: BDF; blue:  $\theta_B$  for  $\delta_c = 2$  cm and for different values of the subreflector eccentricity;  $e$ , at 77 GHz.

a chip generates multiple beams within an offset compatible with the targeted applications, i.e.  $\pm 1$  degree. The main reflector is paraboloidal, with focal distance and diameter  $F$  and  $D$ , respectively. The main steps of the Cassegrain reflector design are reported as follows.

The first step for the antenna system design is the definition of the Cassegrain geometry, which depends on the unit cell dimension,  $m_a$ , and tilt angle  $\theta_B$ . The Cassegrain reflector, as shown in Fig. 2, consists of a main paraboloidal reflector and a hyperbolical subreflector having one of its focal points coinciding with the focal

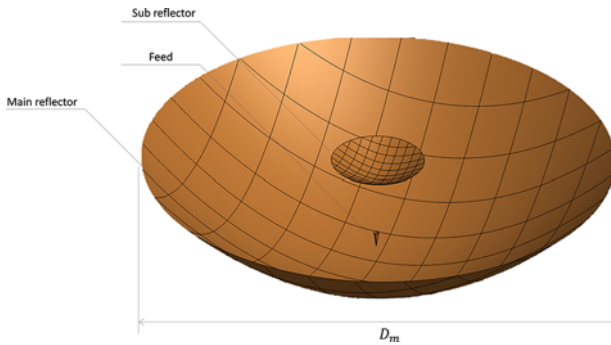


Figure 4. Cassegrain simulation test setup using physical optics.

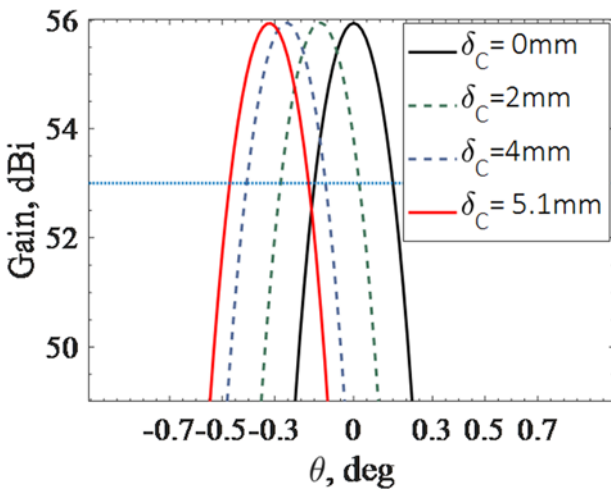


Figure 5. Cassegrain gain as a function of the lateral feed displacement,  $\delta_c$ .

point of the main reflector. The main design parameters are defined as follows:

- $D_m$ : diameter of the main reflector;
- $F_m$ : focal length of the main reflector;
- IF: distance between the focal points of the subreflector;
- $e$ : eccentricity of the subreflector.

The feed phase center should be ideally placed on the second focal point of the hyperboloidal subreflector. Under these conditions, the gain of the reflector is optimal, and the beam pattern is fully symmetric. As the feed is laterally displaced from the focus, a phase taper in the subreflector is created, which in turn leads to a tilted beam. The relation between the feed offset angle,  $\theta_F$ , and the resulting tilted beam direction,  $\theta_B$ , is called beam deviation factor (BDF), and its expression can be approximated as [13, 14]:

$$\text{BDF} = \frac{\theta_B}{\theta_F} = \frac{(4F_m/D_m)^2 + 0.36}{(4F_m/D_m)^2 + 1}. \quad (1)$$

The BDF is a function of the main reflector geometry, which approaches 1 as  $F_m/D_m$  approaches infinity (flat plate). For Cassegrain reflectors, the lateral feed movements,  $-\delta_c$ , should be reduced by a magnification factor, which takes into account the secondary reflector effect, and it is defined as:

$$M = \frac{e + 1}{e - 1} \quad (2)$$

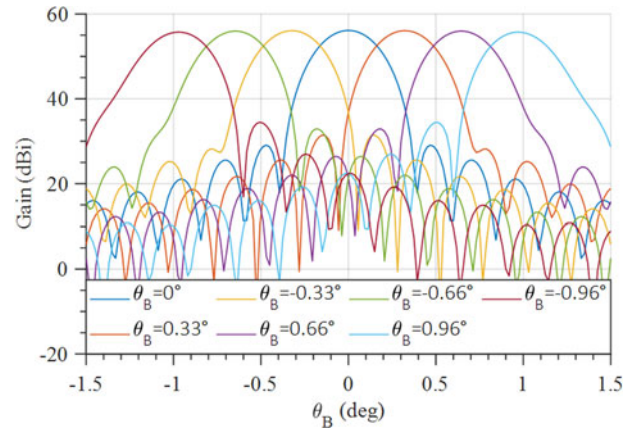


Figure 6. Preliminary Cassegrain double reflector with a horn as reference antenna at @77 GHz.

where  $e$  is the eccentricity of the secondary reflector. If the Cassegrain feed is laterally displaced by  $\delta_c$ , this will correspond to a shift of  $-\delta_c/M$  in the equivalent parabolic reflector.

As it can be observed in Fig. 3, for a given lateral displacement of the feed,  $\delta_c$ , the resulting beam tilt angle,  $\theta_B$ , strongly depends on  $F_m/D_m$  and on the eccentricity of the subreflector,  $e$ . Reducing the subreflector eccentricity results in a higher magnification factor,  $M$ , which in turn decreases the beam tilt,  $\theta_B$ . On the other hand, the feed axial displacement should comply with the feed taper and to its implementation using a planar radiator having size  $m_a \times m_a$  (Fig. 2b). Typically, reflector feeds are designed to achieve a  $-10$  dB taper in correspondence to the reflector border so that spillover losses are kept to a minimum. However, in the case of feed arrays, the axial displacement should be taken into account, thus increasing such a value which, for the case at hand, was found to be ideal at  $-12$  dB. The angular aperture of the feed, defined in correspondence to the 12 dB taper, is identified as  $\theta_{\text{Feed}}$ .

The Cassegrain configuration was optimized using the configuration shown in Fig. 4 [15] using a horn antenna with  $\theta_{\text{Feed}} = 26$  degree to evaluate the reflector gain and the beam steering effect related to the feed axial displacement. The Cassegrain design was thus optimized to achieve a gain higher than 50 dBi and a feed array cell size,  $m_a$ , compatible with a beam aperture achievable in printed circuit technology. The following geometrical parameters were selected:

- $D_m$ : 90 cm;
- $F_m$ : 22.5 cm;
- IF: 15.7;
- $e$ : 1.7;

These values lead to an  $F_m/D_m = 0.25$ . When the feed is axially symmetric, the antenna gain is equal to 55 dBi and its HPB is equal to 0.33 deg. As it can be observed in Fig. 5, in order to achieve a beam scanning without relevant superpositions between adjacent beams, the feed should be laterally displaced by  $\delta_c = 5.1$  mm. When the feed is located in this position, the beam points at  $-0.15$  deg, which corresponds to half the HPB.

The full scanning range shown in Table 1 can be thus achieved using an array of  $7 \times 7$  feeds having the cell size,  $m_a$ , equal to

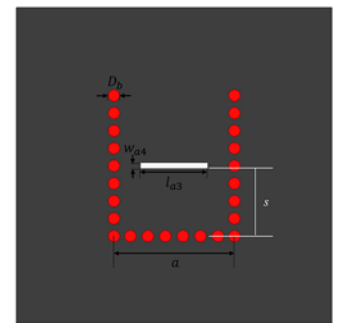
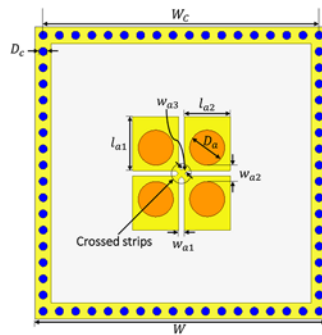
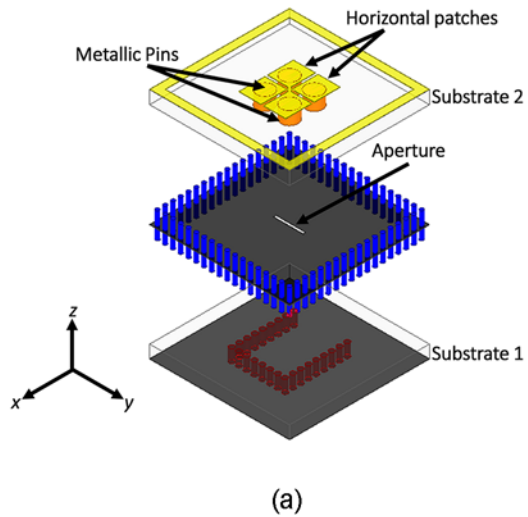


**Figure 7.** Geometry of the SIW-fed aperture-coupled ME dipole antenna: (a) dissection view, (b) top view of Substrate 2, and (c) top view of Substrate 1.

(b)

(c)

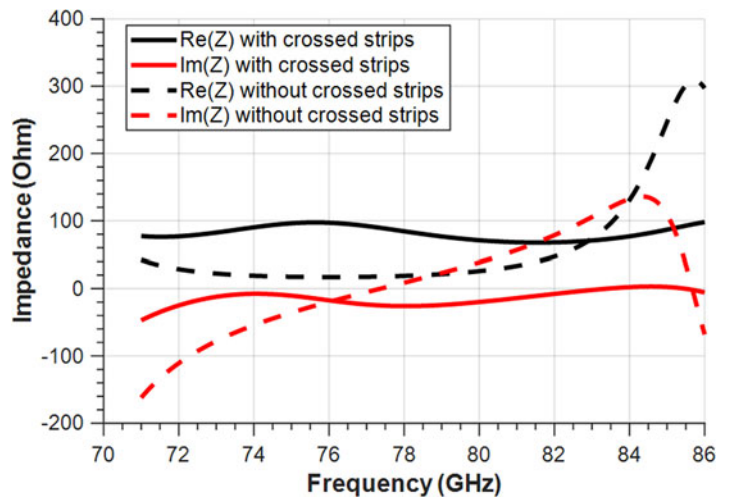


**Figure 8.** Simulated input impedance with and without crossed strips.

5.1 mm. The results obtained with an array of  $7 \times 7$  reference horns simulated using physical optics are shown in Fig. 6. The average gain obtained in this configuration is 56 dBi. In the reference position, the peak gain is 56.12 dBi; at  $0.33^\circ$  of steering, the peak gain is 56 dBi; at  $0.66^\circ$ , the peak gain is 55.95 dBi; and

at  $0.96^\circ$ , the peak gain is 55.66 dBi. As it can be observed, the angle of the main beam does not significantly affect the gain in the other configurations when compared to the reference case, where the antenna is positioned at the reference location. In fact, the maximum loss is estimated to be around 0.5 dB in relation to the

**Table 2.** Parameters of the proposed SIW-fed ME dipole

Parameters	Values (mm)
$W$	5.4
$W_{a1}$	0.1
$W_{a2}$	0.3
$W_{a3}$	0.08
$W_{a4}$	1.2
$W_c$	5.1
$l_{a1}$	1
$l_{a2}$	0.85
$l_{a3}$	1.15
$D_a$	0.65
$D_c$	0.2
$D_c$	0.15
$a$	2.06
$s$	1.2

reference case. Additionally, the level of the side lobes is satisfactory in all configurations.

### Primary feed array design

The main design objective of the present work is the design of a primary feed compatible with Printed Circuit Board (PCB)

technology and providing the required feed taper (i.e.  $\theta_{\text{Feed}} = 26$  degree) fitting within the unit cell size  $m_a \times m_a$ . The unit cell size arising from the physical optics analysis reported in the previous section suggests the use of a unit cell size of 5.1 mm, which corresponds to an aperture of  $1.25 \lambda_0$ . It is worth noticing that the feed elements should have a high inter-element isolation when arranged in the array.

Typically, a single patch antenna would provide a gain limited to about 8 dBi and a bandwidth of 10%, whereas twice this value is required to cover the entire E-band. A first option would be the use of a small array of antennas as reported, for instance, in [16], where a  $2 \times 2$  array of slot-fed patch antennas is reported. The antenna is based on a hybrid feed network, and it occupies an overall size of  $5 \times 5 \times 5$  mm, achieving a gain of about 12 dBi. The gain decreases to 0 dBi at an elevation angle of about 60 deg. A similar gain is achieved in [17] using an antenna in package integrated with a lens. The overall size of this configuration is equal to  $10 \times 10$  mm<sup>2</sup>.

With this configuration, a roll-off of 12 dB is reached at 30 deg. Attempts were also done integrating a pyramidal horn in PCB technology as reported in [18]. However, this antenna requires a complex stack-up while providing a limited gain (i.e. about 9 dBi at 77 GHz). A last relevant example is reported in [19] where a substrate integrated waveguide (SIW) slot antenna array is presented reporting a gain of 12 dBi at 72 GHz. This solution is based on a multilayer PCB configuration, and it provides a bandwidth of 16%.

Hence, the aim of this work is to design and develop a novel feed antenna that meets the specifications for gain and bandwidth, while simultaneously being simple to manufacture and possess a high level of isolation between neighboring feeds. For the case at hand, the design was based on ME dipole antennas [20]. This type of

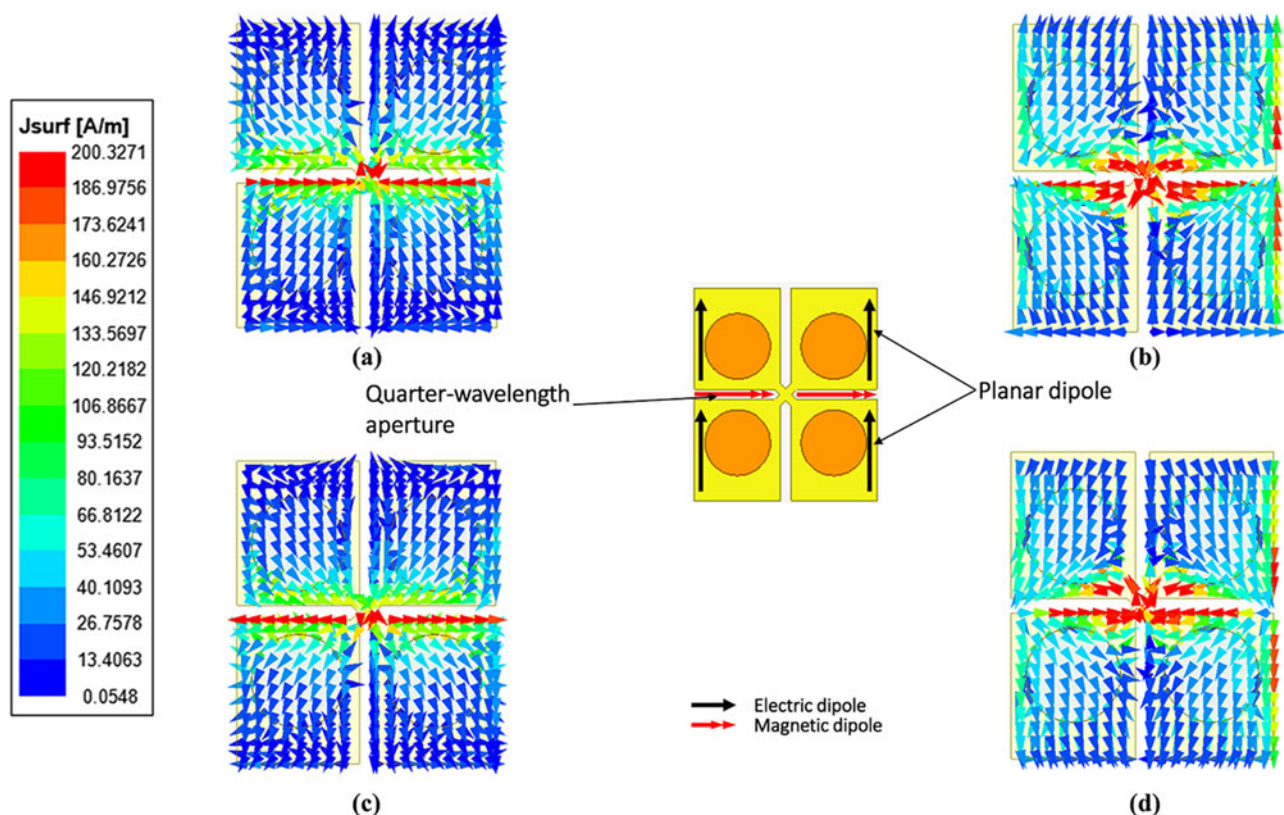


**Figure 9.** Current distributions of the proposed ME dipole at 77 GHz over a period of time: (a)  $t = 0$ , (b)  $t = T/4$ , (c)  $t = T/2$ , and (d)  $t = 3T/4$ .

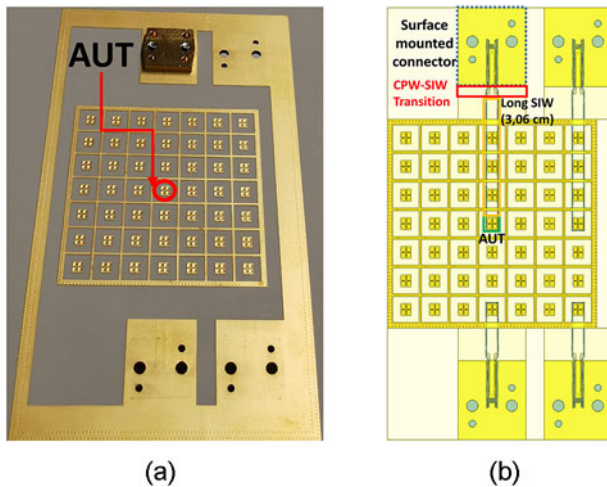
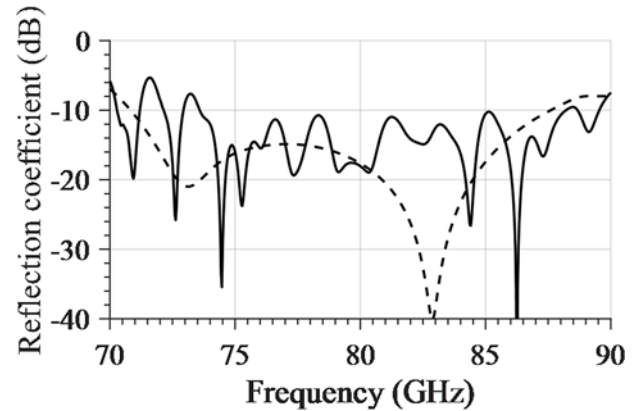


**Figure 10.** Proposed ME dipole in a  $7 \times 7$  feed array configuration: (a) photograph of the prototype and (b) layout of the array board.

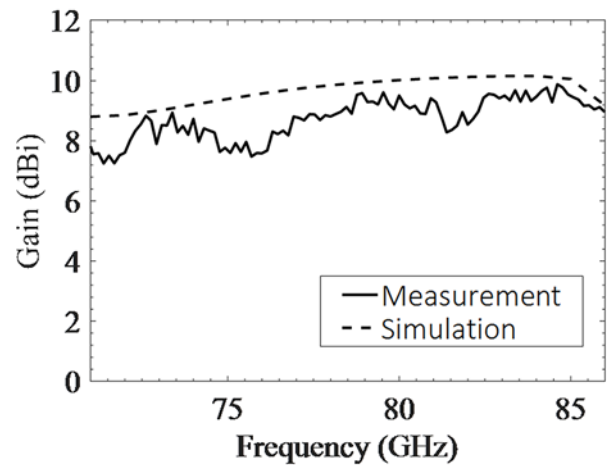
antenna has been recently introduced, and it is receiving a growing attention because of its ease of integration in PCB and wideband properties. ME antennas are a type of antenna that utilize both electric and magnetic fields to generate a symmetrical radiation pattern with low back radiation. These antennas are characterized by their compact size, wide bandwidth, and ability to operate at multiple frequencies [21]. They are typically used in applications such as wireless communications [22], radar, and medical imaging. The unique properties of ME antennas are due to the interaction between the electric and magnetic fields within the antenna, which results in a highly directional radiation pattern.

### Magnetolectric dipole geometry

The proposed ME dipole antenna is designed to match the bandwidth and beam shape requirements derived in section “Beam-switched Cassegrain antenna concept”. The proposed antenna geometry is shown in Fig. 7. The envisioned structure is fed using an aperture-coupling scheme, which has been successfully used for microstrip patch antennas. Specifically, an E-band SIW-fed aperture-coupled ME dipole antenna has been designed, which has good characteristics including wide bandwidth, high radiation efficiency, symmetrical radiation patterns, low back radiation, and low cross-polarizations. The antenna is implemented using only two dielectric layers, referred to as Substrate 1 and Substrate 2 [12]. The dissection view, as illustrated in Fig. 7a, shows that the entire ME dipole is constructed on Substrate 2. This is achieved through a pair of horizontal planar dipoles, which are composed of four identical metallic patch sections that are printed on the top dielectric surface. Each patch is connected to the ground through a vertical metallic via. Additionally, a single aperture having size  $l_{a3} \times w_{a4}$  is etched on the top of the ME dipole ground plane; it is centrally positioned with the ME dipole and excited through an SIW. The width of the SIW, denoted as  $a$ , is chosen to be 2.06 mm in order to ensure that over the operating band the SIW supports only the dominant mode and is also positioned far away from the cut-off frequency. The SIW is terminated with a short circuit located at  $s = 1.2$  mm from the slot border. Furthermore, the diameter of the vias composing the SIW is  $D_b = 0.2$  mm. The size of the ground plane for a single feed is equal to  $W_c = m_a = 5.1$  mm.



(a)



(b)

**Figure 11.** Simulated (dashed) and measured (solid) reflection coefficient (a) and gain (b) of the proposed SIW-fed aperture-coupled ME dipole. The radiating element taken as a reference is the central one.

Furthermore, in order to mitigate the presence of surface waves and to enhance the antenna gain, a via cage has been incorporated on Substrate 2.

All the dielectric layers were implemented by using Rogers 3003 laminates with a thickness of 0.5 mm and a relative permittivity of 3. Therefore, the E-band SIW-fed aperture-coupled ME dipole has an overall height of 1 mm, while the height of the ME dipole is  $0.22 \lambda_g$ , where  $\lambda_g$  is the guided wavelength when  $\epsilon_r = 3$  at 77 GHz. The proposed antenna was simulated using [23], and its geometrical parameters were optimized to provide a uniform gain response and a good matching over the entire bandwidth. As shown in [24], the ME dipole has two resonant frequencies, one related to the magnetic dipole and one to the electric dipole, typically at lower frequency. The wideband performance of the antenna is strongly related to the frequency of these resonances. In general, most of ME dipoles present in literature are fed using a L-probe [25] as with a coupling aperture, and it is difficult to achieve a good impedance matching. For this reason, crossed strips were introduced between the four ME dipole patches. As it can be seen in Fig. 8, the strips introduce an inductive coupling between the patches, which results in an increase of the matching bandwidth. The detailed geometrical parameters are summarized in Table 2. To validate the working mechanism of the proposed aperture-coupled ME dipole antenna, the simulated current distributions are shown in Fig. 9.

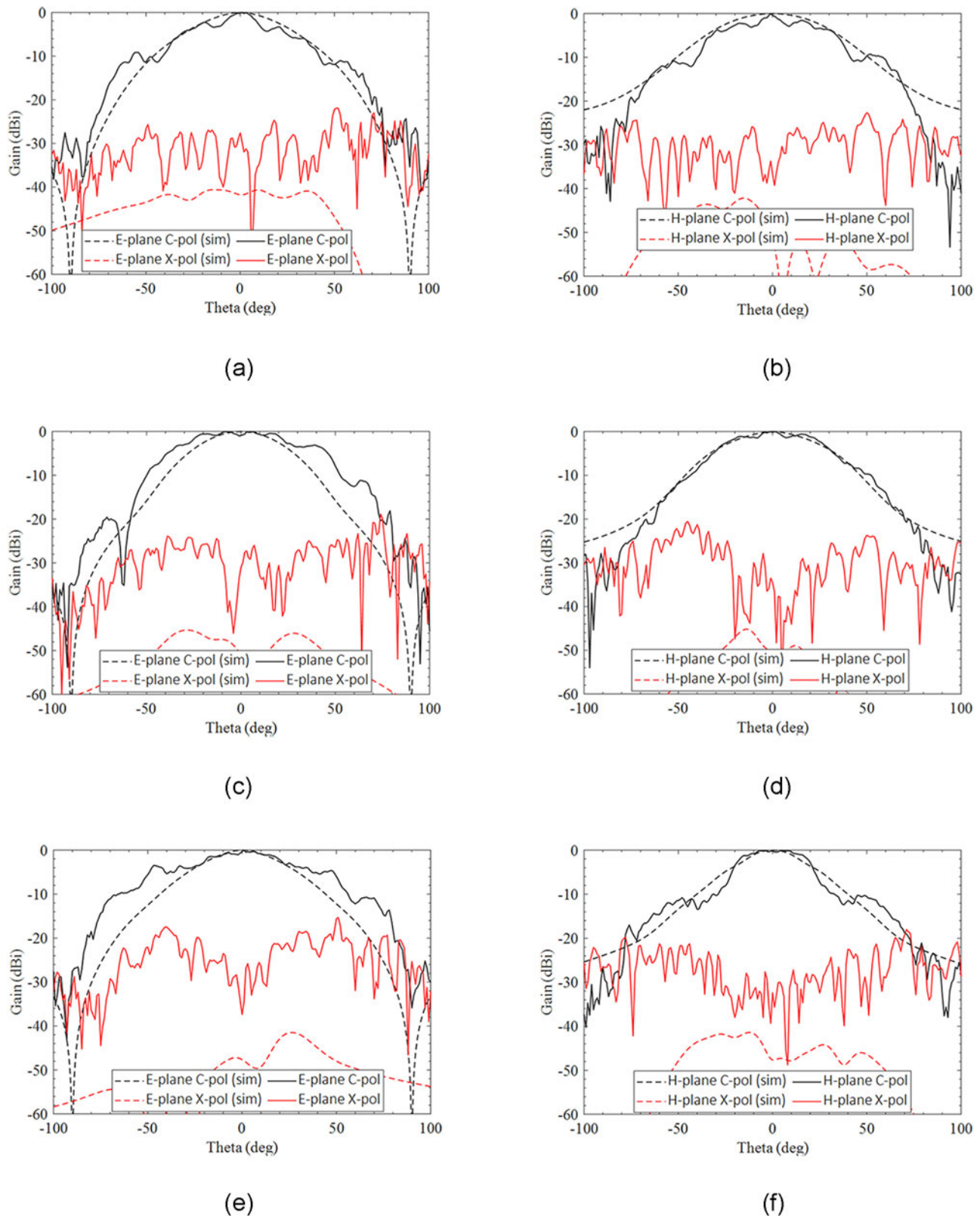


**Figure 12.** Measured and simulated radiation patterns of the central element at (a) 71 GHz E-plane, (b) 71 GHz H-plane, (c) 77 GHz E-plane, (d) 77 GHz H-plane, (e) 85 GHz E-plane, and (f) 85 GHz H-plane.

As can be noticed, at time  $t = 0$  and  $T/2$ , where  $T$  is a period of time, the current on the inner edges of the horizontal patches in  $y$ -direction, are excited. On the other hand, at time  $t = T/4$  and  $3T/4$ , the current is concentrated on the major portion of

apertures, that is to say the equivalent magnetic dipole in  $y$ -direction, are excited. On the other hand, at time  $t = T/4$  and  $3T/4$ , the current is concentrated on the major portion of

**Table 3.** Comparison of E-band antennas for feed array applications

Ref	Gain (dBi)	Aperture size (mm × mm)	Bandwidth GHz	Configuration
[11]	12	5 × 5	76–79	2 × 2 printed array
[17]	12	10 × 10	70–84	Lens antenna
[13]	9	3.5 × 3.5	70–105	Integrated pyramidal horn (6 PCB layers)
[14]	12	6.5 × 6.5	66–78	SIW slot array
This work	9.8	5.1 × 5.1	71–86 (20%)	2 layers PCB

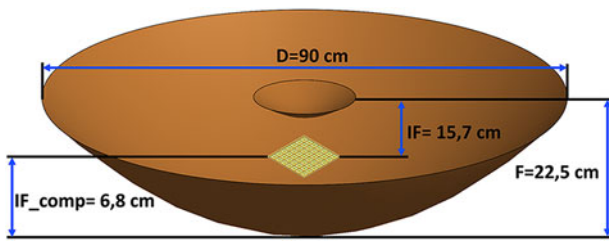


**Figure 13.** Cassegrain antenna fed by 7 × 7 SIW-fed aperture-coupled ME dipole antenna array.

the horizontal patches, which indicates that the electric dipole in *x*-direction is strongly excited. Therefore, the planar electric dipole and the magnetic dipole are excited alternately with similar strength. As mentioned in [20], the combination of the cross-electric and magnetic dipoles acts as a complementary antenna, thus producing the desirable unidirectional pattern with low back radiation.

A design guideline for the proposed antenna (Fig. 7) is given taking into account the most relevant parameters. First, the thickness of the PCB laminate used to design the antenna, that is to say the height of the magnetic dipole, should be chosen around  $0.25\lambda_g$ , where  $\lambda_g$  is the wavelength in substrate at the central frequency of the operating band. Second, there are two resonances over the whole operating band, as shown in Fig. 8, the lower resonance is mainly controlled by the length of the horizontal planar patches  $l_{a1}$ , while the higher one is sensitive to the height of the magnetic dipole. Hereafter, the operating frequency can be tuned by choosing the two dimensions. Third, the diameter of the vertical metallic vias  $w_{a2}$ , the spacing between the vertical metallic vias  $l_{a3}$  can also affect the impedance characteristics of the antenna significantly. By tuning these parameters, a good impedance matching can be obtained.

### Magnetolectric dipole feed array results

The validation of the proposed design concepts was done through the design, fabrication, and test of a 7 × 7 feed array of the ME dipoles with a final dimension of 37.2 × 37.2 mm. The size of the test board exceeds the actual size of the feed array because of the need to find room for the location of the PCB-to-waveguide transitions required for the experimental assessments. A photo of the prototype is shown in Fig. 10(a). Measured results were performed on a subset of four of the 49 elements without relevant differences. Each element under test was connectorized through a waveguide launcher, leaving the other elements unconnected. The simulated coupling between the elements exceeds 40 dB. Experimental results were compared with simulations of the stand-alone array [23].

The reflection coefficient of the proposed antenna is shown in Fig. 11(a). As it can be noticed, the simulated antenna presents a good impedance matching, with a reflection coefficient remaining below -10 dB in the band of interest, from 71 to 86 GHz. The 10 dB fractional bandwidth simulation is greater than 20%. Measurements show similarities, though some variations exist due to connector-induced peaks in the reflection coefficient at lower

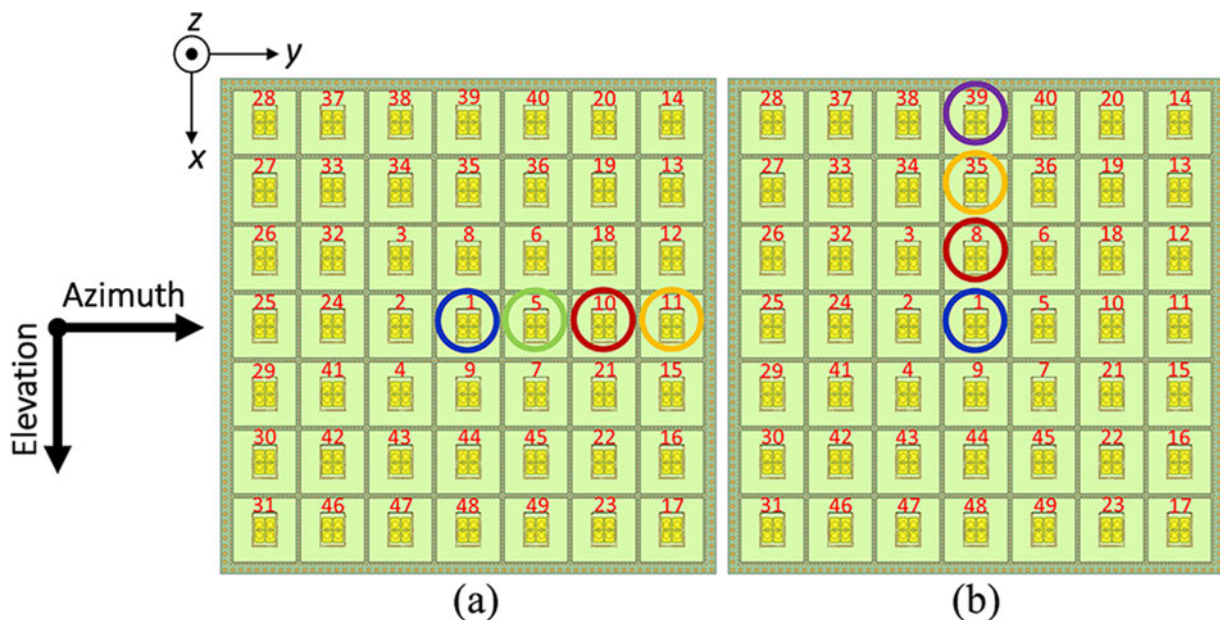
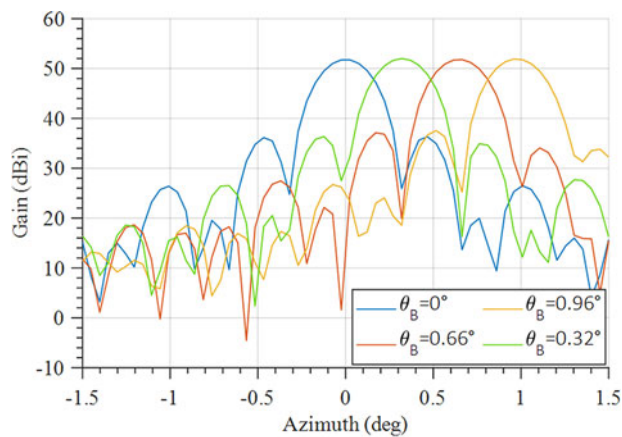
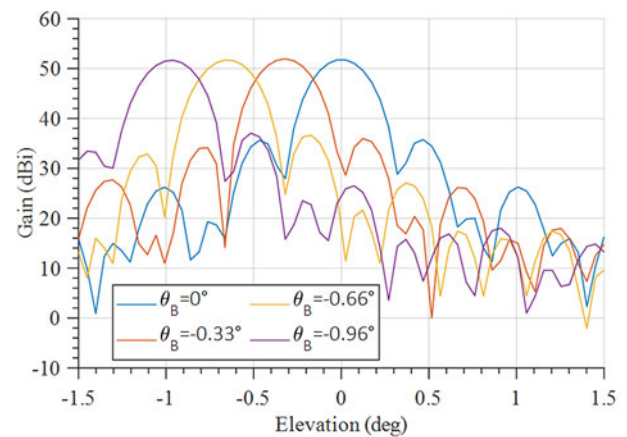


**Figure 14.** 7 × 7 SIW-fed aperture-coupled ME dipole antenna array with the excitation ports activated separately along (a) Azimuth cut and (b) elevation cut.

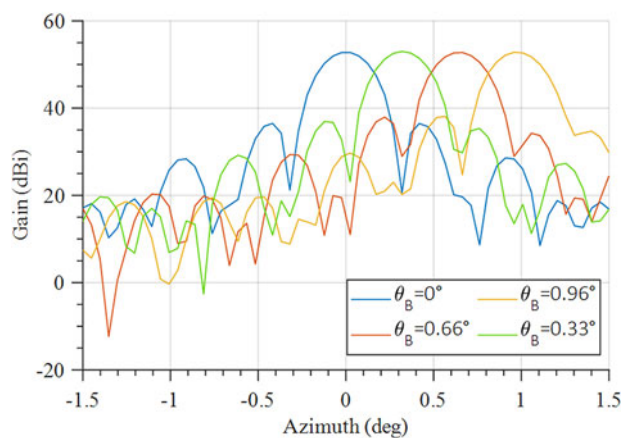




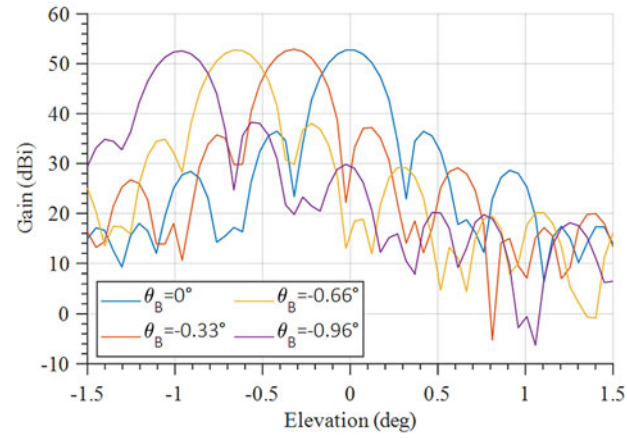
(a)



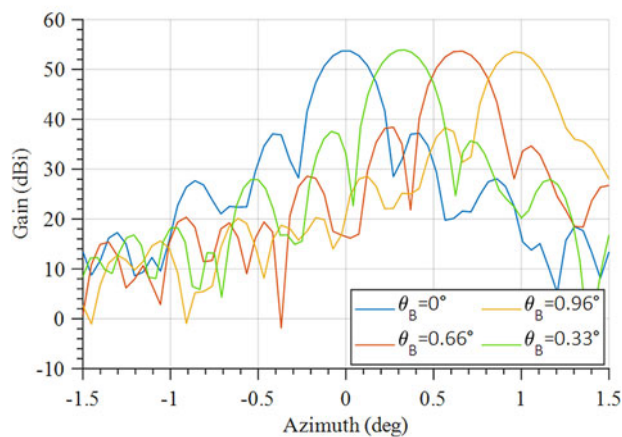
(a)



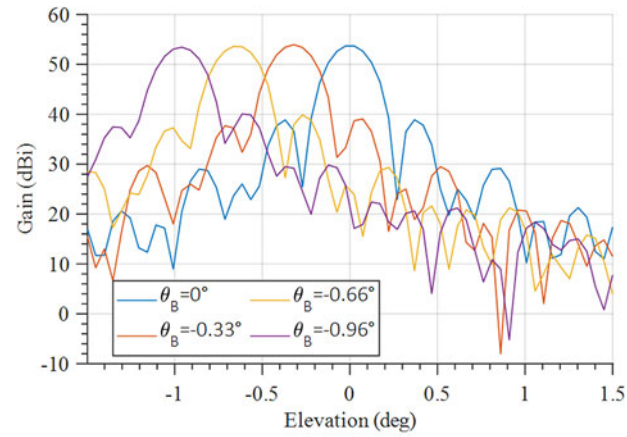
(b)



(b)



(c)



(c)

**Figure 15.** Cassegrain antenna radiation patterns along Azimuth cut by activating separately ports 1, 5, 10, and 11 at (a) 71 GHz, (b) 77 GHz, and (c) 85 GHz.

**Figure 16.** Cassegrain antenna radiation patterns along elevation cut by activating separately ports 1, 8, 35, and 39 at (a) 71 GHz, (b) 77 GHz, and (c) 85 GHz.

frequencies (below 74 GHz and to the use of a 3 cm-long SIW), required to bring the signal out and feed the antenna element. Moreover, a coplanar waveguide to SIW transition was necessary to properly feed the ME dipoles.

The gain response of the proposed antenna is presented in Fig. 11(b), which shows a simulated peak gain of 10 dBi at 84 GHz. The simulated 3-dB beamwidth covers all the band of interest, and

the gain variations remain within 1.4 dBi in the E-band. The measured gain is generally in line with simulations, with a peak gain of 9.8 dBi at 83.8 GHz. The normalized simulated and measured radiation patterns at 71, 77, and 85 GHz are reported in Fig. 12. Both measured and simulation results show a tapered beam with a 12 dB beamwidth reached at about 50 degrees in both cuts with some differences depending on the frequency. Cross-polar levels are below 28 dB while reporting a deterioration in the upper band. The results

of the proposed feed array antenna are compared with other similar relevant configurations in Table 3. As it can be observed, the proposed antenna is the best compromise between gain, area, and manufacturing technology.

### Feed array in Cassegrain configuration

The evaluation of the feed array reported in the previous section was finalized using its simulated results to feed the Cassegrain reflector designed in section “Beam-switched Cassegrain antenna concept”. For this purpose, Ansys Savant [26] was used. The actual Cassegrain configuration which includes the  $7 \times 7$  SIW-fed ME aperture-coupled antenna array and which will be used in Savant is shown in Fig. 13. The Cassegrain evaluation required two steps. First, the full  $7 \times 7$  array was simulated, and results were imported into the Savant environment, which uses physical optics simulation. The simulation setup is reported in Fig. 14.

The complete Cassegrain antenna was analyzed along the azimuth and elevation cuts by activating the elements one by one. The active elements were numbered as reported in Fig. 14. Specifically, ports 1, 5, 10, and 11 were activated to estimate the azimuth scanning, whereas elements 1, 8, 35, and 39 were enabled to assess the elevation scan. Simulated radiation patterns of the feed array Cassegrain reflector are reported in Fig. 15 at three different frequencies, i.e., 71, 77, and 85 GHz. In line with the results observed in Fig. 1, each cell provides a steering angle of approximately 0.33 degrees in both scanning directions. As a consequence,  $\theta_B = 0.33, 0.66,$  and  $0.96$  degrees in both azimuth and elevation scans. At the center band frequency of 77 GHz, a gain of 53 dBi is reached while scan losses are less than 0.25 dB. At the lower and upper edge of the band, the gain peaks are 51.73 and 53.93 dBi, respectively, with similar scan losses (Fig. 16).

### Conclusion

A beam-switching high-gain E-band Cassegrain reflector antenna 5G backhauling systems was presented. The final beam-switched Cassegrain antenna is realized by a  $7 \times 7$  SIW-fed aperture-coupled ME dipole antenna array, which feeds the double-reflector structure and meets all the system requirements. A prototype of the Cassegrain illuminator was prototyped and tested. The simulated results of the proposed feeder element demonstrate a fractional bandwidth of more than 20%, and the proposed antenna achieves the expected results at 71 to 86 GHz. The simulated 3-dB beamwidth covers all the band of interest with a peak gain of 11.2 dBi at 86 GHz, while the measured peak gain is 8.4 dBi at 74 GHz. The discrepancies between measured and simulated data are related to the presence of transitional circuits not de-embedded.

The full Cassegrain antenna demonstrates adequate impedance matching, with values remaining below  $-10$  dB over the entire E-band. The average peak gain for the antenna surpasses 52 dBi throughout the entire bandwidth. The antenna's beam can be directed within an angular deviation of  $\theta_B = \pm 1^\circ$  in all planes, with each component of the feed array capable of tilting the main beam by an angle of  $\theta_B = \pm 0.33^\circ$ . The performance of the proposed configuration compares favorably to that of a horn-based feed array, offering the added advantage of being easier to integrate with front-end modules.

**Acknowledgement.** Antenna patterns were characterized at the Politecnico di Torino (Italy).

**Funding statement.** This work was supported by European ECSEL/JU/EUH2020 under grant TARANTO “Towards Advanced BiCMOS NanoTechnology Platforms for RF and THz Applications” (no. 737454).

**Competing interests.** The authors report no conflict of interest.

### References

1. Amendola G, Boccia L, Centurelli F, Chevalier P, Fonte A, Mustacchio C, Pallotta A, Tommasino P, Traversa A and Trifiletti A (2021) Compact E-Band I/Q receiver in SiGe BiCMOS for 5G backhauling applications. *IEEE Transactions on Circuits and Systems II: Express Briefs* 68(9), 3098–3102.
2. Rzaa J (2012) Pointing, acquisition, and tracking for directional wireless communications networks. Available at <https://drum.lib.umd.edu/handle/1903/14195> (accessed 5 February 2023).
3. Kalimulin R, Artemenko A, Maslennikov R, Putkonen J and Salmelin J (2015) Impact of mounting structures twists and sways on point-to-point millimeter-wave backhaul links. In *2015 IEEE International Conference on Communication Workshop (ICCW)*. 19–24.
4. Chaloun T, Boccia L, Arnieri E, Fischer M, Valenta V, Fonseca NJ and Waldschmidt C (2022) Electronically steerable antennas for future heterogeneous communication networks: Review and perspectives. *IEEE Journal of Microwaves* 2(4), 545–581.
5. Ala-Laurinaho J, Aurinsalo J, Karttunen A, Kaunisto M, Lamminen A, Nurmiharju J, Räisänen AV, Säily J and Wainio P (2016) 2-D beam-steerable integrated lens antenna system for 5G E-band access and Backhaul. *IEEE Transactions on Microwave Theory and Techniques* 64(7), 2244–2255.
6. Bisognin A, Cihangir A, Luxey C, Jacquemod G, Pilard R, Giancesello F, Costa JR, Fernandes CA, Lima EB, Panagamuwa CJ and Whittow WG (2016) Ball grid array-module with integrated shaped lens for wigig applications in eyewear devices. *IEEE Transactions on Antennas and Propagation* 64(3), 872–882.
7. Plastikov AN (2016) A high-gain multibeam bifocal reflector antenna with  $40^\circ$  field of view for satellite ground station applications. *IEEE Transactions on Antennas and Propagation* 64(7), 3251–3254.
8. Wang J, Zhou Y, Xia H and Zhi Yang X (2017) Design of a high-isolation 35/94-GHz dual-frequency orthogonal-polarization cassegrain antenna. *IEEE Antennas and Wireless Propagation Letters* 16, 1297–1300.
9. Rotman W and Turner R (1963) Wide-angle microwave lens for line source applications. *IEEE Transactions on Antennas and Propagation* 11(6), 623–632.
10. Säily J, Pokorný M, Kaunisto M, Lamminen A, Aurinsalo J and Raida Z (2016) Millimetre-wave beam-switching rotman lens antenna designs on multi-layered LCP substrates. In *2016 10th European Conference on Antennas and Propagation (EuCAP)*. 1–5.
11. Ramanujam P, Rao SK, Vaughan RE and McCleary JC (1999) Reconfigurable multiple beam satellite reflector antenna with an array feed. EP0963005A2. Available at <https://patents.google.com/patent/EP0963005A2/en> (accessed 24 December 2022).
12. Mustacchio C, Boccia L, Arnieri E, Scalise G and Amendola G (2022) E-band SIW-fed aperture coupled magneto-electric dipole antenna for 5G backhauling systems. In *2022 Microwave Mediterranean Symposium (MMS)*. 1–4.
13. Milligan TA (2005) *Modern Antenna Design: 1*, 2nd edn. Hoboken, NJ: IEEE.
14. Lo Y (1960) On the beam deviation factor of a parabolic reflector. *IRE Transactions on Antennas and Propagation* 8(3), 347–349.
15. TICRA (2022) GRASP | Reflector antenna design software. Available at <https://www.ticra.com/software/grasp/> (accessed 5 February 2023).
16. Qiu Y and Li B (2020) E-band microstrip patch array antenna based on hybrid feeding network. In *2020 International Conference on Microwave and Millimeter Wave Technology (ICMMT)*. 1–3.
17. Tong Z, Fischer A and Maurer L (2013) Radiation performance enhancement of E-Band antenna in Package. *IEEE Transactions on Components, Packaging, and Manufacturing Technology* 3(11), 1953–1959.

18. **Ghassemi N and Wu K** (2012) Millimeter-wave integrated pyramidal horn antenna made of multilayer Printed Circuit Board (PCB) process. *IEEE Transactions on Antennas and Propagation* **60**(9), 4432–4435.
19. **Aliakbari H, Mosalanejad M, Soens C, Vandebosch GAE and Lau BK** (2019) Wideband SIW-based low-cost multilayer slot antenna array for 5G-band applications. *IEEE Transactions on Components, Packaging, and Manufacturing Technology* **9**(8), 1568–1575.
20. **Luk K-M and Wu B** (2012) The magnetolectric dipole – a wideband antenna for base stations in mobile communications. *Proceedings of the IEEE* **100**(7), 2297–2307.
21. **Mak K-M, So -K-K, Lai H-W and Luk EK-M** (2017) A magnetolectric dipole leaky-wave antenna for millimeter-wave application. *IEEE Transactions on Antennas and Propagation* **65**(12), 6395–6402.
22. **Li Y and Luk K-M** (2016) 60-GHz dual-polarized two-dimensional switch-beam wideband antenna array of aperture-coupled magneto-electric dipoles. *IEEE Transactions on Antennas and Propagation* **64**(2), 554–563.
23. (2022) ANSYS HFSS | 3D high frequency simulation software. Available at <https://www.ansys.com/products/electronics/ansys-hfss> (accessed 5 February 2023).
24. **Luk K-M and Wong H** (2006) A new wideband unidirectional antenna element. *International Journal of Microwave and Optical Technology* **1**(1), 35–44.
25. **Li M and Luk K-M** (2015) Wideband magneto-electric dipole antenna for 60-GHz millimeter-wave communications. *IEEE Transactions on Antennas and Propagation* **63**(7), 3276–3279.
26. (2022) ANSYS savant technical features. Available at <https://www.ansys.com/it-it/products/electronics/ansys-savant-technical-features> (accessed 5 February 2023).



**Carmine Mustacchio** was born in Crotona, Italy, in 1993. He received the M.S. degree in Telecommunications Engineering and the Ph.D. in Information and Communication Technologies from the University of Calabria, Rende, Italy, in 2017 and 2021, respectively. In 2021, he was a Research Fellow with the MAIC lab with the Department of Informatics, Modeling, Electronics and System Engineering, University of Calabria, Italy. In 2022, he joined the CEA-Leti Technology Institute, Grenoble, France, where he worked as Antenna Research Engineer. He is currently

an Antenna System Designer with ST Microelectronics, Grenoble, France. His research interests include millimeter-wave antennas for 5G applications and gain enhancement techniques for on-chip antennas in SiGe BiCMOS technology.



**Emilio Arnieri** was born in Cosenza, Italy, in 1977. He received the Degree (Hons.) in Information Technology Engineering from the University of Calabria, Rende, Italy, in 2003, and the Ph.D. degree in Electronics Engineering from the University Mediterranea of Reggio Calabria, Reggio Calabria, Italy, in 2007. He is currently an Assistant Professor with the Department of Informatics, Modeling, Electronics and System Engineering, University of Calabria, where he has participated in several national, European Union,

and ESA projects. He has coauthored more than 90 articles published in international journals and proceedings of international conferences. His research interests include circular polarizers, the development of dual-band antennas and millimeter-wave components, synthetic aperture radar, and beam scanning antennas. He is an Associate Editor for *IEEE Antennas and Wireless*

*Propagation Letters*, an Advisory Editor for the *Wiley Engineering Reports*, and a Guest Editor for *MDPI Sensors* and *MDPI Electronics*. He is the Co-Founder of the academic spinoff Antecnica. Dr. Arnieri was selected as a finalist for the Best Paper Award in Antenna Design at the 13th European Conference on Antennas and Propagation (EuCap 2019).



and Integrated Circuits (MAIC) Laboratory. His current research interests include antennas, phased arrays, and microwave and mm-wave circuits. He was responsible for numerous research projects funded by the European Union and the European Space Agency.

**Giandomenico Amendola** received the M.Sc. degree in electrical engineering from the University of Calabria, Rende, Italy, in 1987. From 1988 to 1992, he was a Research Fellow with the Proton Synchrotron Division, European Center for Nuclear Research, Geneva, Switzerland. He is currently a Full Professor with the Department of Informatics, Modeling, Electronics and System Engineering, University of Calabria, where he is also the Director of the Millimeter-wave Antennas



point radio link applications. He has authored several papers in peer-reviewed international journals and conference proceedings and two book chapters. He is the SIAE contact person for European and ESA projects.

**Alessandro Fonte** was born in 1980. He received M.S. degree and Ph.D. in Electronic Engineering at the University of Pisa (Italy), in 2005 and 2008, respectively. Since 2011, he has been with the SIAE Microelettronica S.p.A. (Milan, Italy), where he is a Senior Microwave Engineer and Member of the Technical Staff. His current research interests include the design of micro- and millimeter-wave system-on-chip front-ends in silicon and III-V semiconductor technologies for point-to-



point radio link applications. He has authored several papers in peer-reviewed international journals and conference proceedings and two book chapters. He is the SIAE contact person for European and ESA projects.



Antenna Handbook (Wiley, 2012). His current research interests include active antennas, reflectarrays, beam-scanning antennas, and microwave and mm-wave IC design. Dr. Boccia is a member of the European Microwave Association (EuMA) and the Società Italiana di Elettromagnetismo (SIEm). He serves as an Associate Editor for the *IEEE Microwave and Wireless Components Letters* and the *International Journal of Microwave and Wireless Technologies* (Cambridge University Press).

**Luigi Boccia** was born in Lungro, Italy, in 1975. He received the Ph.D. degree in Electronics Engineering from the University of Calabria, Rende, Italy, in 2000, and the Ph.D. degree in Electronics Engineering from the University Mediterranea of Reggio Calabria, Reggio Calabria, Italy, in 2003. From 2005 to 2021, he was an Assistant Professor in electromagnetics with the University of Calabria, where he is currently an Associate Professor. He is the Coeditor of the *Space*